Available online at www.sciencedirect.com
ScienceDirect
Journal of Nuclear Materials 374 (2008) 422–430
journal of nuclear materials
www.elsevier.com/locate/jnucmat

Effect of Si and Zr on the interdiffusion of U–Mo alloy and Al

Jong Man Park [a,*], Ho Jin Ryu [a], Seok Jin Oh [a], Don Bae Lee [a], Chang Kyu Kim [a], Yeon Soo Kim [b], G.L. Hofman [b]

[a] *Korea Atomic Energy Research Institute, Daedeokdaero 1045, Yuseong, Daejeon 305-353, Republic of Korea*
[b] *Argonne National Laboratory, 9700 S. Cass Avenue, Argonne, IL 60439, USA*

Received 15 May 2007; accepted 14 September 2007

Abstract

We investigated the effect of Zr additions to U–Mo and Si additions to Al on interdiffusion between U–Mo and Al by employing diffusion couple tests. We examined the phase stability of the γ-heat-treated alloys by high-temperature annealing tests. Using X-ray diffraction, we observed that the γ-phase U–7Mo–Zr alloys with more than 2 wt% Zr decomposed faster than the U–7Mo alloys. The diffusion couples showed that a Zr addition to U–7Mo and the addition of Si in Al reduced the interaction layer growth rates. However, Zr additions to U–Mo are most effective in reducing the overall interdiffusion rates when combined with Si additions to Al. The decomposition of the metastable U–Mo γ-phase during the diffusion test appears to have a significant effect on the overall interdiffusion rates.

1. Introduction

U–Mo/Al dispersion fuel is being developed as a high-uranium-density fuel for high performance research reactors due to its excellent stability during irradiation [1]. Although it meets all other fuel requirements, the further development of this fuel was delayed due to an unacceptable volume expansion caused by (U–Mo)–Al interaction layer (IL) formation and a subsequent gross pore formation at the interface between U–Mo and matrix Al [2].

In the literature, diffusion couple tests between U and Al have shown that a Si addition to Al reduces the IL growth rate [3]. In addition, there were studies that tried Si additions in U–Al dispersion fuel to suppress UAl_4 formation during the high-temperature fabrication process [4,5]. To the early U–Al fuel developers, UAl_4 was known as a brittle compound that must be avoided to improve fuel fabricability. On an analogous base in the previous literature, the Si-modification of the Al matrix in U–Mo/Al dispersion fuel was recently proposed at ANL to solve the gross pore formation problem mentioned above [6].

Previous out-of-pile diffusion studies have shown that Si indeed accumulates in the IL between U–Mo and Al–Si [7,8]. In-pile tests also showed the positive effect of Si: the IL thickness was much thinner than in the fuel plates using a pure Al matrix, and no porosity was formed [9,10]. Tests of rod-type fuel elements containing U–Mo/Al–Si dispersion fuel are under way [11].

Zirconium was identified as another element with the potential to stabilize the IL when added to U–Mo alloy rather than Al [6,12]. Before irradiation tests were performed, out-of-pile tests were selected to confirm the effects of Zr additions to the fuel with or without Si added in the Al matrix. We performed diffusion-couple tests between U–Mo–*x*Zr and Al–*y*Si with various contents of Zr and Si. This paper presents the results from these diffusion-couple tests. The results revealed that both the Zr addition to U–7 wt% Mo and the Si addition to Al, either simultaneously or separately, suppressed the growth of the ILs. We also found that, when Zr was added to fuel, the accumulation of Si, originally added in Al, was enhanced in the IL.

* Corresponding author.
E-mail address: jmpark@kaeri.re.kr (J.M. Park).

0022-3115/$ - see front matter © 2007 Elsevier B.V. All rights reserved.
doi:10.1016/j.jnucmat.2007.09.059

2. Experimental procedures

For the diffusion-couple tests, we fabricated U–7 wt% Mo–xZr ($x = 0, 1, 2, 4$ wt%) alloys by using a vacuum-induction melting in a zirconia crucible. The as-cast U–7Mo–xZr ingots were then heat-treated in a vacuum at 950 °C for 24 h and sequentially water-quenched to stabilize the γ-U phase. Stabilities of the γ-phase of the U–Mo–xZr alloys were compared by using X-ray diffraction (XRD) after an annealing at 500 °C from 10 min to 48 h. The clamped U–7Mo–xZr vs. Al–ySi ($y = 0, 2, 5$ wt%) diffusion couples were annealed at 580 and 600 °C from 1 to 10 h in a vacuum-sealed fused quartz tube. The test temperatures 580 and 600 °C were selected mainly because we wanted to investigate diffusion behaviors between U–Mo–Zr and Al–Si in the $\alpha + \gamma$ phase and close to the $\gamma/\alpha + \gamma$ phase boundary of U–Mo alloy. At these high temperatures, the clamp pressure effect on diffusion-couple tests becomes negligible due to softening of Al.

Microstructures of the interaction layers (ILs) in the diffusion-couple test specimens were examined with an optical microscope and a scanning electron microscope (SEM). Concentration profiles of the ILs were measured with the electron probe micro-analysis (EPMA) method.

3. Results

3.1. γ-Phase stability

Fig. 1 shows that the γ-heat-treated U–7Mo–xZr alloys consist of a metastable isotropic γ-U (cubic) phase, irrespective of the Zr content. The γ-phase U–7Mo–xZr alloys annealed at 500 °C transformed to a mixture of the α-U phase and the γ′-U_2Mo phase which is the equilibrium phase composition below ~600 °C for a U–7Mo alloy. Fig. 2 compares the effects of a Zr addition on the relative stability of the γ-phase for the U–7Mo–xZr ternary alloys.

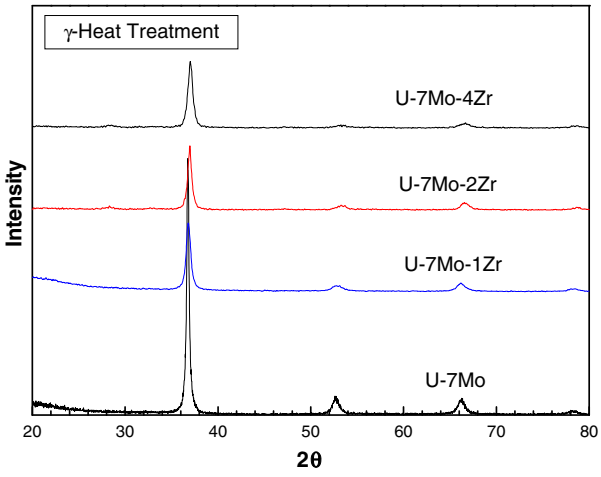

Fig. 1. X-ray diffraction patterns of the γ-heat-treated U–7Mo–xZr at 950 °C for 24 h.

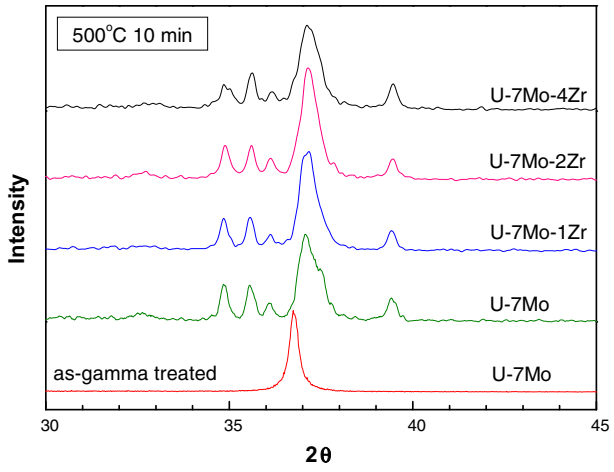

(a) Anneal for 10 min.

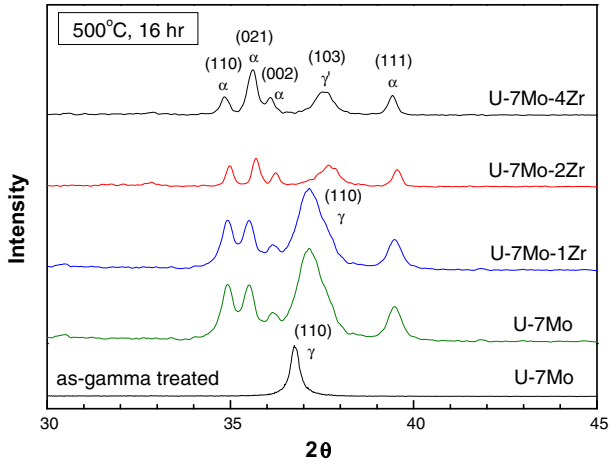

(b) Anneal for 16 h.

Fig. 2. X-ray diffraction patterns showing the transformation of the γ-phase in the U–7Mo–xZr annealed at 500 °C.

Even after 10 min of an annealing at 500 °C, the U–7Mo–xZr alloys show virtually the same diffraction patterns as the transformed U–Mo alloys as shown in Fig. 2(a). This means that the γ-phase U–7Mo decomposes at this temperature so fast that a Zr addition does not influence the initial stage of the decomposition. It is known that U–Mo alloy has a greater degree of thermal stability than U–Zr [13], and the effect of a Zr addition on the γ-phase U–Mo is to decrease the γ-phase stability of U–Mo alloys [14,15]. This was observed for a longer annealing test as shown in Fig. 2(b), in which there are distinct diffraction peaks for the (1 0 3) planes of the γ′-phase in the U–7Mo–2Zr and U–7Mo–4Zr samples annealed for 16 h. This result confirms that a Zr addition to U–7Mo generally reduces the γ-phase stability and the transformation rate increases as the Zr content increases. The SEM images of the decomposed γ-phase after an annealing test (48 h) are shown in Fig. 3. The transformed microstructures of U–7Mo–2Zr and U–7Mo–4Zr are too fine to identify their phase evolution.

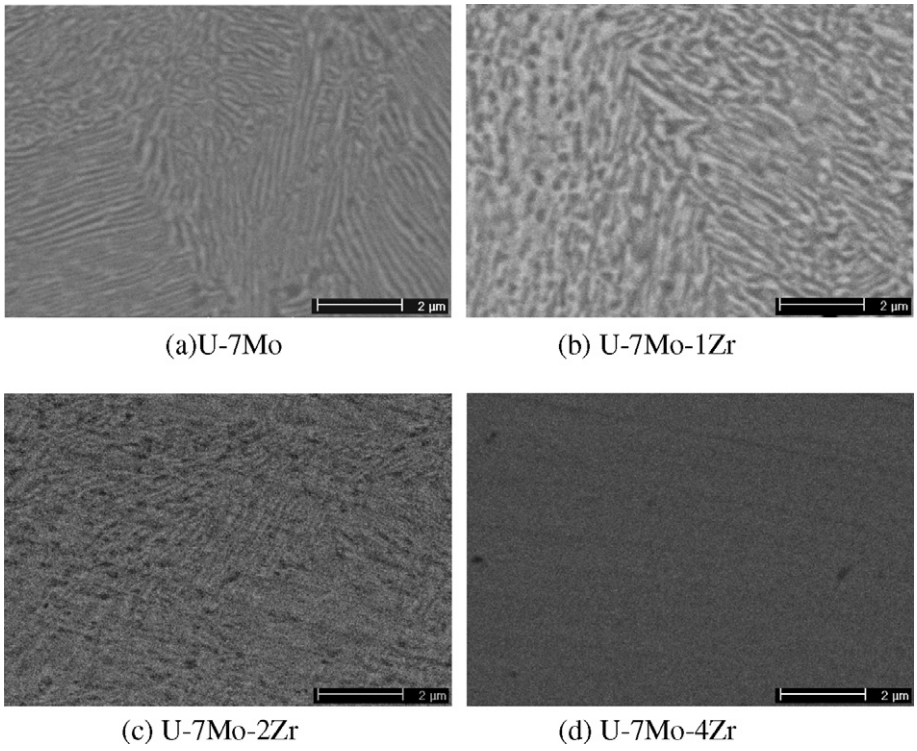

Fig. 3. SEM images of the U–7Mo–*x*Zr alloys after an annealing at 500 °C for 48 h.

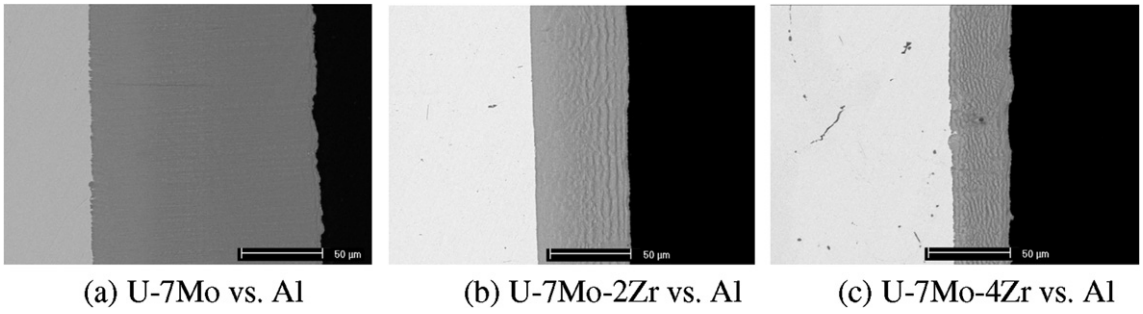

Fig. 4. SEM images of diffusion couples after an annealing at 580 °C for 5 h.

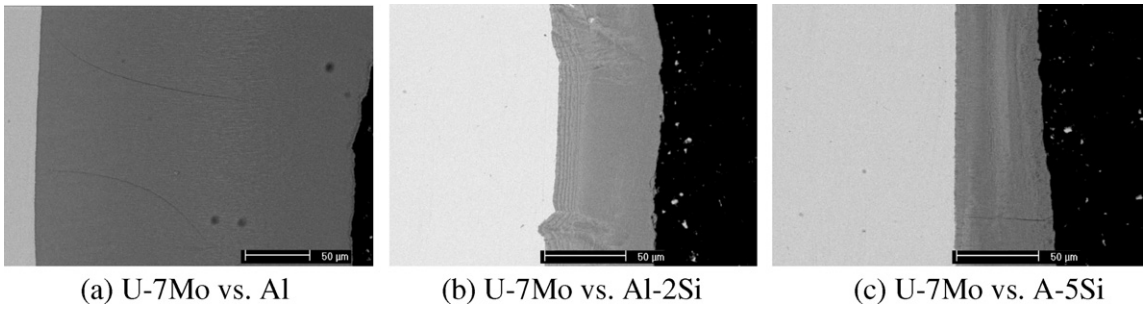

Fig. 5. SEM images of diffusion couples after an annealing at 600 °C for 3 h.

3.2. Microstructural analysis and growth of the interaction layers

The IL thickness data for U–7Mo–*x*Zr vs. Al diffusion couples annealed at 580 °C for 5 h are compared in Fig. 4. The IL thickness decreased significantly as the Zr content increased; ~140, ~60 and ~40 μm for 0, 2 and 4 wt%, respectively. The formation of a multi-phase structure in the IL becomes more prominent as the Zr content increases.

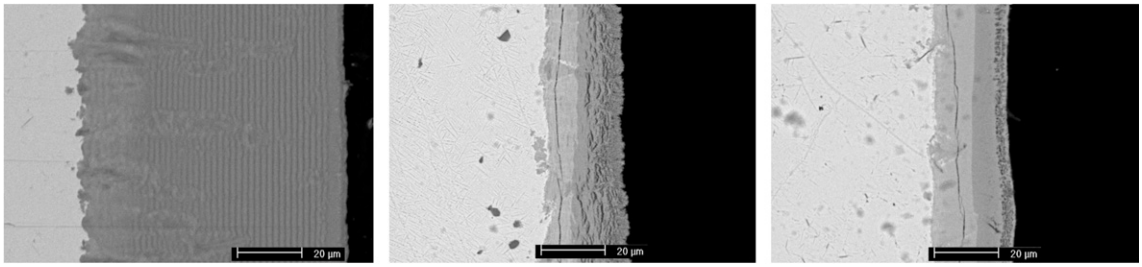

(a) U-7Mo-4Zr vs. Al (b) U-7Mo-4Zr vs. Al-2Si (c) U-7Mo-4Zr vs. Al-5Si

Fig. 6. SEM images of diffusion couples after an annealing at 600 °C for 3 h.

Table 1
Measured IL thicknesses of U–Mo–Zr vs. Al–Si diffusion couples

	U–7Mo		U–7Mo–2Zr		U–7Mo–4Zr	
	580 °C 5 h	600 °C 3 h	580 °C 5 h	600 °C 3 h	580 °C 5 h	600 °C 3 h
Al (μm)	135	240	60	240	35	80
Al–2Si (μm)	25	65	30	45	30	25
Al–5Si (μm)	35	63	35	38	32	20

When comparing U–7Mo vs. Al–*y*Si diffusion couples annealed at 600 °C for 3 h with respect to the Si composition (y) as shown in Fig. 4, we found that the IL thickness decreased considerably from ~240 μm for U–7Mo/Al to ~65 μm for U–7Mo/Al–2Si. However, the increase in the Si–content beyond 2% did not decrease with the IL thickness further as is shown in the case for U–7Mo/Al–5Si. From Figs. 4 and 5, it appears that the effectiveness in suppressing the IL growth rate of a 4% Zr addition to U–7Mo in U–7Mo/Al is similar to that of a 2% Si addition to Al in U–7Mo/Al.

The diffusion couple of U–7Mo–4Zr vs. Al–5Si showed the thinnest IL (~20 μm), as shown in Fig. 6. The effect of Si addition in Al on an IL thickness reduction seemed to be enhanced when Zr was simultaneously added to U–7Mo. The combined effects are presented in Table 1.

3.3. Compositional analysis of IL

We measured the constituent concentrations in the ILs of the diffusion couples by using the EPMA method. In Figs. 7–9, the concentration distribution profiles are superimposed on the corresponding micrographs of the ILs. The U–7Mo–*x*Zr ($x = 0$, 2, and 4) vs. Al diffusion couples annealed at 600 °C for 3 h shown in Fig. 7 exhibited similar profiles for U, Mo, Zr, and Al in the ILs. The Al-to-(U + Mo) ratio increased from the U–Mo side to the Al side of the ILs, which has a chemical composition similar to UAl_4, whereas the Zr-to-U ratio remained constant throughout the ILs. In the U–7Mo–4Zr vs. Al diffusion couple shown in Fig. 7(c), a striated multilayer morphology is clearly visible in the ILs, which is a feature often observed in multi-component diffusion couples [16].

Preferential accumulation of Si in the interaction products of the U–Mo/Al–Si diffusion couples was observed, as demonstrated in Fig. 8, in which the position of the peak Si accumulation in the IL moved to the U–Mo side as the Si content in the Al–Si increased. This is consistent with the theoretical prediction [8] and the out-of-pile test results [9,10]. When Zr was added to U–Mo, however, we found a noticeable difference in both the microstructure and Si distribution as shown in Fig. 9(b) and (c). A multi-phase structure formed along the IL of the U–7Mo–4Zr/Al–Si diffusion couples. A high-Si accumulation (~60 at.% Si) was also found in the layer on the U–Mo–Zr side. The composition of this layer was similar to that of $U(Al,Si)_2$ and this phase was quietly different from that observed in the previous result [7], in which the composition of $(U,Mo)(Al,Si)_3$ with 57 at.% of Si was observed along the IL of the U–7Mo/A356 (containing 7.1 wt% of Si) diffusion couple at 340 °C.

Fig. 10 compares the diffusion paths in the ternary phase diagrams for the U–Mo vs. Al–Si and U–Mo–Zr vs. Al–Si diffusion couples. They are contrastingly different from each other because the U–Mo vs. Al–Si diffusion couple formed an IL with the Al/(U + Mo) ratio of ~3 whereas the U–Mo–Zr vs. Al–Si diffusion couples formed an IL with the Al/(U + Mo) ratio of ~2. Since Zr is the only difference, we deduced that Zr facilitated in the formation of the lower Al content compound in the IL. Because an interaction compound with an Al-to-(U + Mo) ratio less than 4 is favored due to its stability [6], this result can give a positive sign for irradiation tests.

The atomic ratios of (Al + Si) to (U + Mo + Zr) are compared in Fig. 11 for all the test cases. In this figure, we see that (i) Zr addition to U–Mo regardless of the Zr

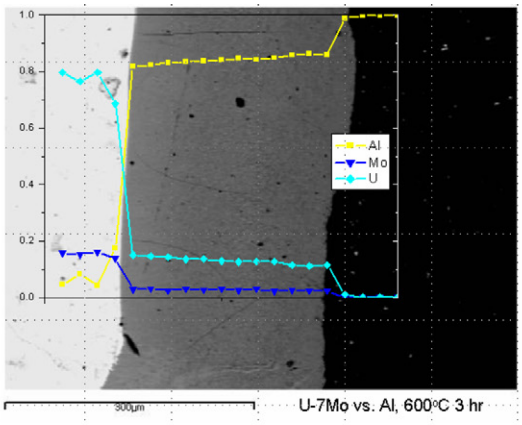

(a) U-7Mo vs. Al

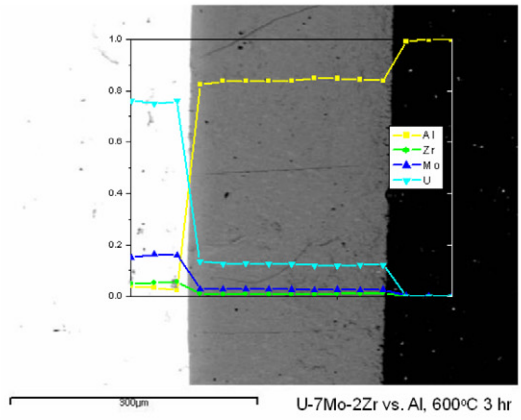

(b) U-7Mo-2Zr vs. Al

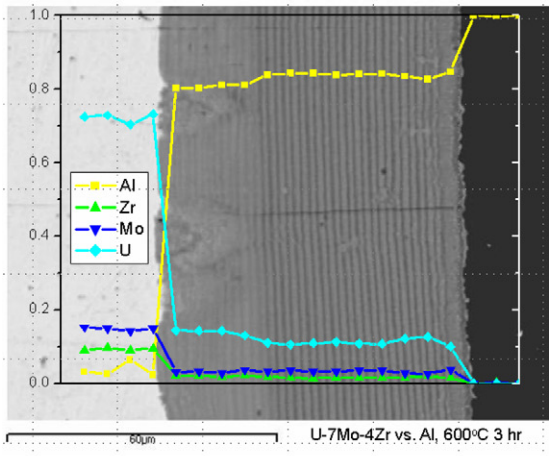

(c) U-7Mo-4Zr vs. Al

Fig. 7. Compositional profiles of ILs from diffusion couples annealed at 600 °C for 3 h.

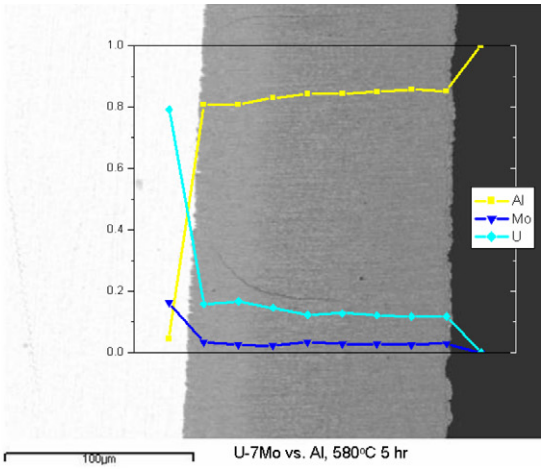

(a) U-7Mo vs. Al

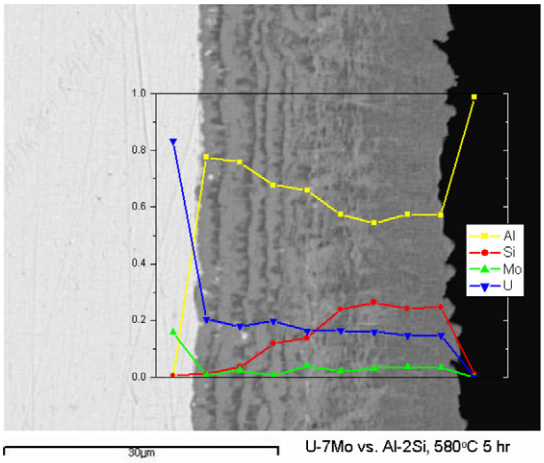

(b) U-7Mo vs. Al-2Si

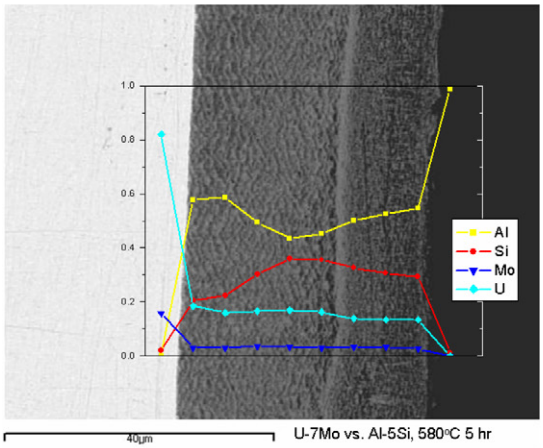

(c) U-7Mo vs. Al-5Si

Fig. 8. Compositional profiles of ILs from diffusion couples annealed at 580 °C for 5 h.

content, and without a Si addition to Al, does not reduce the Al-to-(U + Mo) ratio of the interaction product below 4. (ii) The Si addition to Al with or without a small amount of Zr addition to U–Mo can reduce the ratio to below 4. (iii) The best result can be obtained from U–7Mo–2Zr vs. Al–5Si diffusion couples.

4. Discussion

As mentioned in Section 3.1 above the metastable γ-phase, which is the initial condition of the U–Mo part

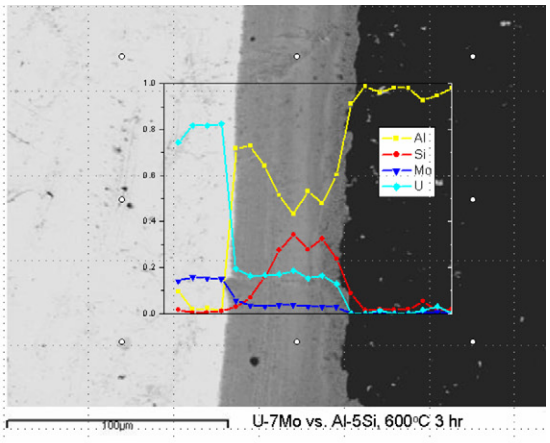

(a) U-7Mo vs. Al-5Si

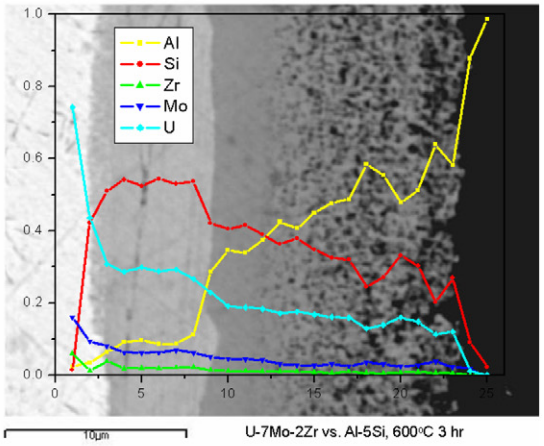

(b) U-7Mo-2Zr vs. Al-5Si

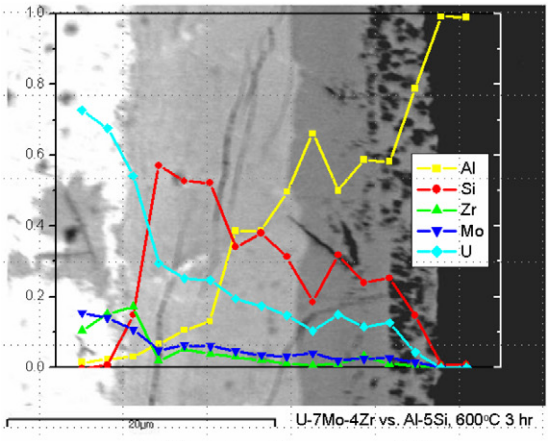

(c) U-7Mo-4Zr vs. Al-5Si

Fig. 9. Compositional profiles of ILs from diffusion couples annealed at 600 °C for 3 h.

of all diffusion couples, will tend to transform to its two-phase equilibrium depending on temperature, time and Mo concentration. When comparing the interdiffusion rates for various experimental conditions, one should be mind-full of the effect of this phase transformation on the interdiffusion kinetics.

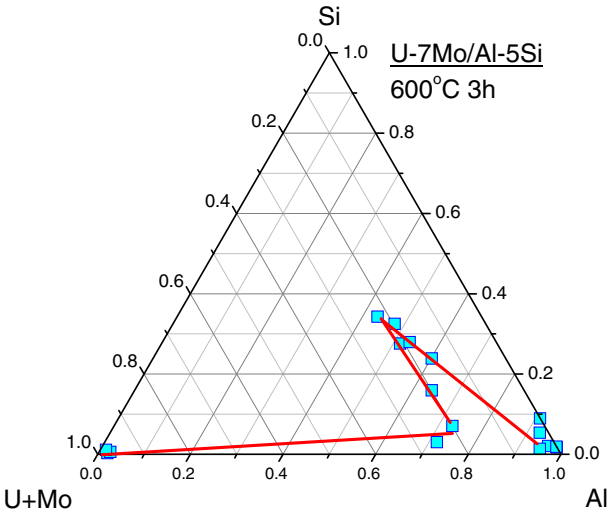

(a) U-7Mo/Al-5Si

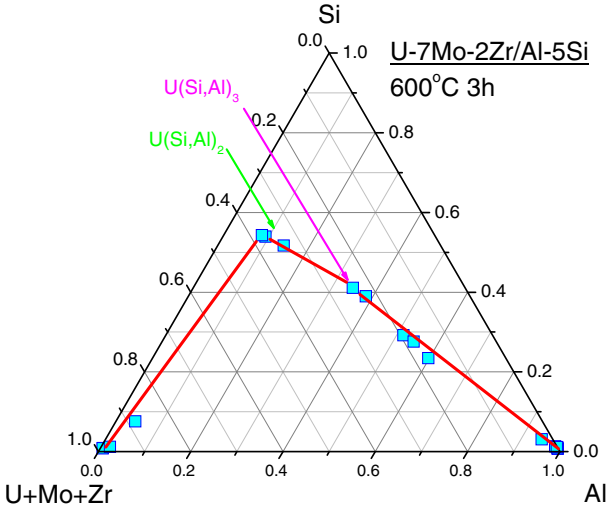

(b) U-7Mo-2Zr/Al-5Si

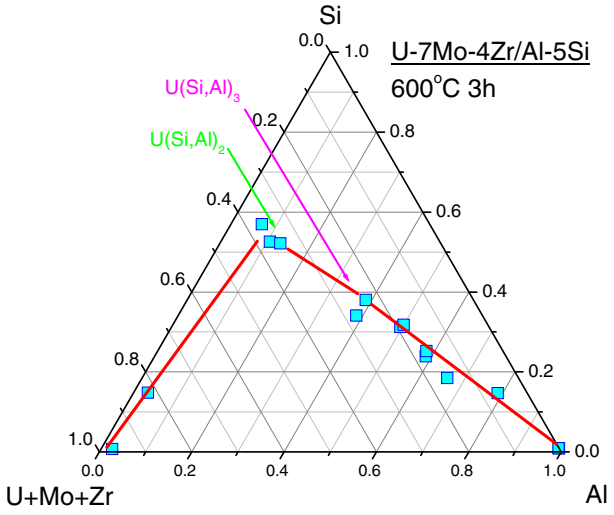

(c) U-7Mo-4Zr/Al-5Si

Fig. 10. Comparison of diffusion paths for diffusion couples annealed at 600 °C for 3 h.

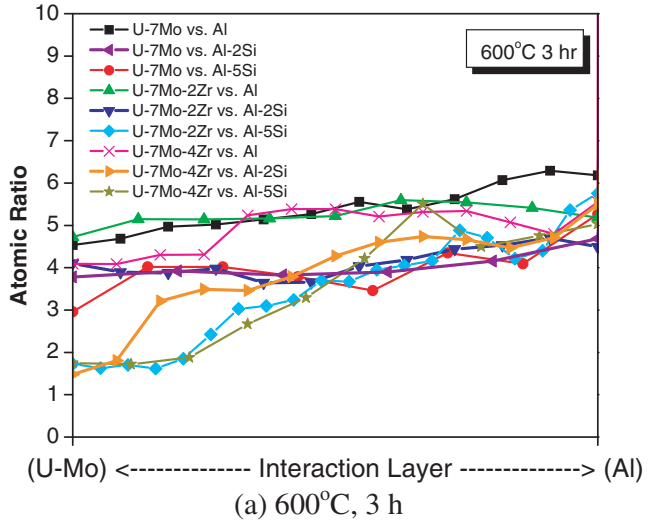

Fig. 11. (Al + Si)/(U + Mo + Zr) ratios measured across the ILs for the U–7Mo–*x*Zr vs. Al–*y*Si diffusion couples.

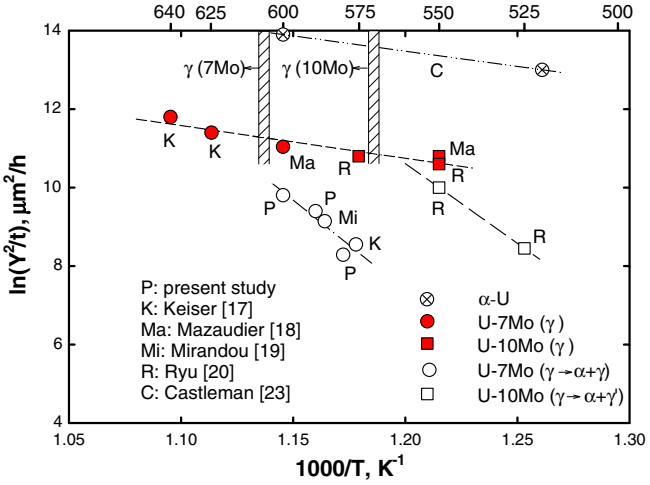

Fig. 12. Comparison of diffusivity data in the literature. The γ-phase boundaries for U–7Mo and U–10Mo alloys are also shown. The temperature and composition of the data included in this figure are shown on the U–Mo phase diagram in Fig. 13.

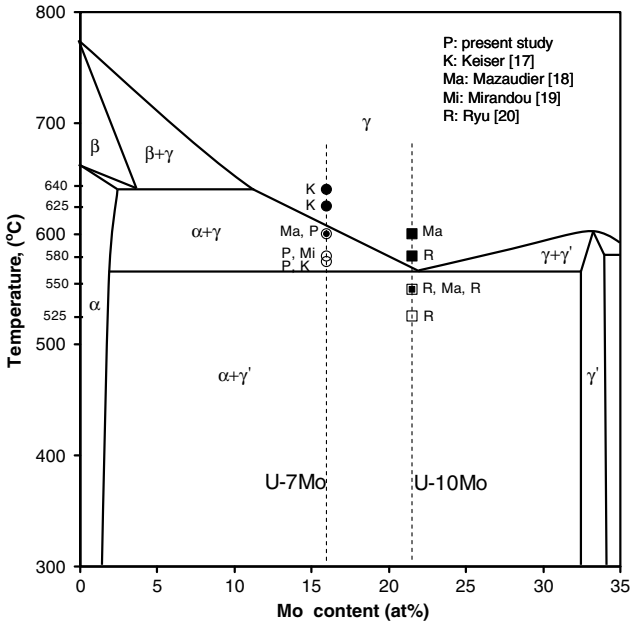

Fig. 13. U–Mo phase diagram [22] and composition and temperature for the data included in Fig. 12.

Before further assessing the effect of Zr and Si on the interdiffusion behavior we have examined available data on U–Mo/Al diffusion-couple experiments from several authors [17–20]. The data are shown in an Arrhenius plot (Fig. 12) of $\ln(Y^2/t)$ vs. T^{-1} where Y is the total interdiffusion zone width in μm, t in h of the diffusion anneal and T in K. Only data from samples having regular-planar interdiffusion zones were considered. At first glance, the data appear to be rather inconsistent. However, these apparent inconsistencies can be reconciled when, as shown in Fig. 12, we consider whether, and for how long, the test was performed in either the equilibrium γ-phase or the two-phase fields. The data from samples for which the U–Mo alloy remained as γ-phase during the diffusion anneal (filled symbols in Fig. 12) can be reasonably fit with a straight line. The difference between U–10Mo and U–7Mo is not discernable; this is probably consistent with the ratio of the interdiffusivity in U–Mo at 850 °C, which was measured as only ~1.6 over the composition range [21]. The data represented by the open symbols are from samples for which the U–Mo alloy has transformed to various degrees. The broken lines through these points do not suggest the temperature dependence of the interdiffusion per se, but rather some combination of the kinetics of the phase transformation and the U–Mo/Al interdiffusion. Unraveling these effects would require extensive experimentation which is beyond the scope of the present paper. It appears clear, however, that the interdiffusion rates are drastically reduced and have much stronger temperature dependence with respect to the interdiffusion of Al and γ-phase U–Mo. This is particularly the case for U–7Mo

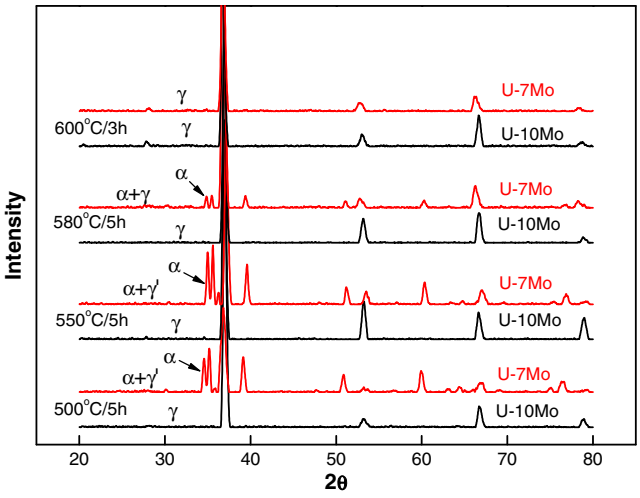

Fig. 14. X-ray diffraction patterns for U–7Mo and U–10Mo.

which transforms rather rapidly as shown by the X-ray diffraction patterns in Fig. 14. Although we do not have long-time diffraction data for U–10Mo, the literature data [15,23] indicate that the longer-time interdiffusion data in Fig. 12 should have been affected by the partial transformation of the U–Mo alloy.

It seems counter intuitive that, with the presence of α-U in the transformed U–Mo alloy, the rate of interdiffusivity should decrease. As shown by the α-U/Al data [24] in Fig. 12, the interdiffusivity with α-U is much higher than with γ U–Mo. It seems that the interdiffusivity is controlled by either the high Mo γ′-phase or, most likely, the fine lamellar morphology of the two-phase structure. This effect (of transformed microstructure), if it is indeed controlling the interdiffusion, should be more pronounced when Zr is present as this has a strong effect on the lamellar morphology as shown in Fig. 3. However, the presence of Zr in the IL, albeit at relatively low concentrations, does have a pronounced effect on the diffusion behavior of Si. As the concentration profiles indicate Si diffusion 'up', its concentration gradient is enhanced in the presence of Zr to the point of formation of a high Si phase at the U–Mo side of the IL, indicating an increased chemical potential gradient for Si. It should be very informative to extend the present study including diffusion tests with Si and Zr in the γ-phase region.

5. Conclusions

(1) Zr addition to U–7Mo reduced the γ-phase stability of the U–Mo alloy and the rate of $\gamma \rightarrow \alpha + \gamma'$ transformation increased as the Zr content increased beyond 2 wt%, with progressively finer lamellar two-phase microstructure.

(2) Diffusion-couple tests showed that a Zr addition to U–7 wt% Mo reduced the IL growth rates progressively with the Zr content until a Zr content of 4% and increased the temperature dependence.

(3) A Si addition to Al had a similar effect on reducing the IL growth as the Si content increases and the maximum was found at 2 wt% in Al.

(4) Zr addition to U–Mo was most effective in reducing the IL growth in combination with Si added to Al. The interaction product formed in a U–Mo–2Zr vs. Al–5Si diffusion couple tested at 580 °C showed that the interaction product formed at or near the U–Mo–Zr/IL interface had the Al/(U + Mo) ratio of ~2.

Acknowledgments

This study was mainly supported as a National Nuclear Research Program by the Ministry of Science and Technology of Korea (MOST). The contribution from Argonne National Laboratory was supported by the US Department of Energy, Office of Global Threat Reduction (NA-21), National Nuclear Security Administration, under Contract No. DE-AC-02-06CH11357 between UChicago Argonne, LLC and the Department of Energy.

References

[1] J.L. Snelgrove, G.L. Hofman, M.K. Meyer, C.L. Trybus, T.C. Wiencek, Nucl. Eng. Des. 178 (1997) 119.
[2] A. Leenaers, S. Van den Berghe, E. Koonen, C. Jarousse, F. Huet, M. Trotabas, M. Boyard, S. Guillot, L. Sannen, M. Verwerft, J. Nucl. Mater. 335 (2004) 39.
[3] L.S. DeLuca, H.T. Sumsion, KAPL-1747, Knolls Atomic Power Laboratory, 1957.
[4] J.E. Cunningham, R.E. Adams, in: Fuel Elements Conference, Paris, November 18–23, 1957, TID-7546, October 31, 1958, p. 102.
[5] J.E. Cunningham, R.J. Beaver, W.C. Thurber, R.C. Waugh, in: Fuel Elements Conference, Paris, November 18–23, 1957, TID-7546, October 31, 1958, p. 269.
[6] Y.S. Kim, G.L. Hofman, H.J. Ryu, J. Rest, in: Proceedings of the 2005 RERTR International Meeting, Boston, USA, November 6–10, 2005. http://www.rertr.anl.gov.
[7] M. Mirandou, S. Arico, L. Gribaudo, S. Balart, in: Proceedings of the 2005 RERTR International Meeting, Boston, USA, November 6–10, 2005. http://www.rertr.anl.gov.
[8] J.M. Park, H.J. Ryu, G.G. Lee, H.S. Kim, Y.S. Lee, C.K. Kim, Y.S. Kim, G.L. Hofman, in: Proceedings of the 2005 RERTR International Meeting, Boston, USA, November 6–10, 2005. http://www.rertr.anl.gov.
[9] Y.S. Kim, G.L. Hofman, H.J. Ryu, M.R. Finlay, D. Wachs, in: Proceedings of the 2006 RERTR International Meeting, Cape Town, South Africa, October 29–November 2, 2006. http://www.rertr.anl.gov.
[10] M. Ripert, S. Dubois, P. Boulcourt, S. Naury, P. Lemoine, in: Transactions of the 10th International Topical Meeting on RRFM, ENS, Sofia, Bulgaria, 2006.
[11] C.K. Kim, K.H. Kim, J.M. Park, H.J. Ryu, Y.S. Lee, D.B. Lee, S.J. Oh, H.T. Chae, C.G. Seo, C.S.Lee, in: Proceedings of the 2005 RERTR International Meeting, Boston, USA, November 6–10, 2005. http://www.rertr.anl.gov.
[12] H.E. Exner, G. Petzow, Metall 23 (1969) 220.
[13] H.A. Saller, R.F. Dickerson, W.E. Murr, Uranium Alloys for High-Temperature Application, BMI-1098, Battelle Memorial Institute, 1956.

[14] G.L. Hofman, M.K. Meyer, A.E. Ray, in: Proceedings of the 1998 RERTR International Meeting, Sao Paulo, Brazil, October 18–23, 1998. http://www.rertr.anl.gov.
[15] C.A.W. Peterson, et al., UCRL-7824, TID-4500, 34th Ed., University of California, National Technical Information Service, US DOC, 1964.
[16] A.A. Kodentsov, M.R. Rijnders, F.J.J. Van Loo, Acta Mater. 46 (1998) 6521.
[17] D.D. Keiser, Argonne National Laboratory Report, ANL-05/14, July, 2005.
[18] F. Mazaudier, C. Proye, F. Hodaj, in: Transactions of the 10th International Topical Meeting on RRFM, Sofia, Bulgaria, ENS, April 30–May 3, 2006.
[19] M. Mirandou, S.N. Balart, M. Ortiz, M.S. Granovsky, J. Nucl. Mater. 323 (2003) 29.
[20] H.J. Ryu, Y.S. Han, J.M. Park, S.D. Park, C.K. Kim, J. Nucl. Mater. 321 (2003) 210.
[21] Y. Adda, J. Philibert, in: Proceedings of the Second United Nations International Conference Peaceful Uses of Atomic Energy, vol. 6, Geneva, United Nations, 1958, p. 1160.
[22] S.P. Carg, J.R. Ackermann, J. Nucl. Mater. 64 (1977) 265.
[23] J.S. Lee, C.H. Lee, K.H. Kim, V. Em, J. Nucl. Mater. 306 (2002) 147.
[24] L.S. Castleman, J. Nucl. Mater. 3 (1) (1961) 1.